In the light of potential applications [1-4] and in objectives of the present work, La(III), Ce(III), Pr(III), Nd(III) and Sm(III) complexes with 2-acetylpyridine acetoylhydrazone (APAH) are synthesized characterized based on physico-chemical techniques and spectral methods viz., IR, UV-Visible spectroscopy. Electrochemical properties of all complexes are studied by cyclic voltammetry. Binding interactions of metal complexes with calf-thymus DNA are carried out using absorption spectroscopy. DNA cleavage activities of the complexes are investigated using gel electrophoresis experiments. The X-Ray crystal structure determination of Ce(III) and Sm(III) complexes of APAH are major highlights in this Chapter.

Synthesis and characterization of APAH (Fig 5.1) are given in Chapter 2. The ligands are synthesized by using corresponding precursors.

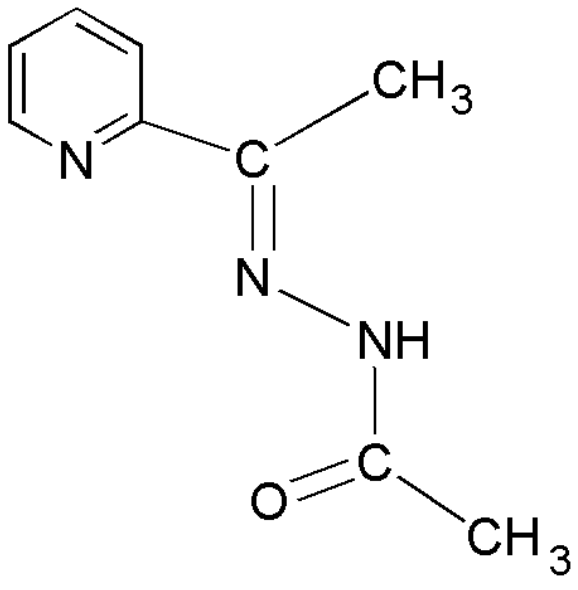

Fig 5.1: The structure of APAH

a. Physico-chemical properties

Syntheses of lanthanide(III) complexes are given in Chapter-2 (Section 2 iii). All the complexes are stable at room temperature, non-hygroscopic, less soluble in water, more soluble in methanol, ethanol and readily soluble in CH_3CN, DMF and DMSO. The analytical data are consistent with the proposed molecular formulae of complexes. Physical properties viz., colour of the complex, melting points and percentage of yield are given in **Table 5.1.**

b. Conductivity measurements

All the complexes are freely soluble in dimethylformamide (DMF), hence the solutions of these metal complexes were prepared in DMF to perform conductivity measurements. Conductivity values of the solutions of the complexes are measured at room temperature. Molar conductivity data suggest that the complexes are 1:2 electrolytes [5, 6]. Molar conductivity data are given in **Table 5.1**.

Table 5. 1 Colors, analytical data, molar conductivities and melting points of the APAH ligand and its Lanthanide(III) complexes

Compound	**Colour**	**M.P °C**	**Yield %**	**Found (cal %)**			Λ_M^*
				C	**H**	**N**	
APAH	White	90-92	74	61.32(61)	6.50(6.25)	24.0(23.71)	
$[La(APAH)_2(NO_3)(H_2O)_2]2NO_3.\ 3H_2O$	White	223-225	69	28.19(28.17)	4.17(4.19)	16.4(16.37)	128
$[Ce(APAH)_2(NO_3)(H_2O)_2]2NO_3.\ H_2O$	Dark yellow	231-233	71	29.42 (29.43)	3.87(3.84)	17.14(17.16)	135
$[Pr(APAH)_2(NO_3)(H_2O)_2]2NO_3.\ 3H_2O$	Ligtht green	235-238	69	27.99 (28.1)	4.2(4.18)	16.3(16.32)	132
$[Nd(APAH)_2(NO_3)(H_2O)_2]2NO_3.3H_2O$	Baby pink	227-229	70	27.97(27.98)	4.18(4.16)	16.24(16.25)	140
$[Sm(APAH)_2(NO_3)(H_2O)_2]2NO_3.\ 2H_2O$	White	210-212	65	28.36 (28.34)	3.95 (3.96)	16.51(16.52)	124

***Units , (Ω^{-1} cm^2 mol^{-1})**

c. Electronic spectra

Lanthanide complexes exhibit various colours due to the redistribution of electrons in the partially filled f-orbitals and referred as f-f transitions. In absence of the ligands around the metal, the energy, of all seven f-orbital's of a lanthanide metal ion are equal and are degenerate. The presence of ligands will result in splitting in the energy levels of these orbital's. In metal complexes some orbitals will interact more strongly than others. The exact form of interaction and energies of f-orbitals depend on the arrangements of ligands around the metal ions. In UV-visible, near IR region of electromagnetic radiation, the transition associated with electronic energy levels of the complexes under investigation can be identified. The electronic spectral data of lanthanide complexes are recorded in dimethyl formamide (DMF).

Electronic spectrum of the free ligand (APAH) in UV region shows an intense band at 298 nm and weaker band at 379 nm which are assigned to the $\pi \rightarrow \pi^*$ and $n \rightarrow \pi^*$transition respectively. These are slightly shifted to higher or lower energy levels in absorption spectra of the lanthanide complexes. In visible region the electronic spectrum of Pr(III), Nd(III), Sm(III) complexes show several important f-f spectral bands, shown in Fig. 5. 2. The electronic spectra of the lanthanide complexes in the visible region exhibit red shift (Fig. 5.3) of all the f-f spectral bands relative to the corresponding Ln(III) aqua ion. The shifts have been attributed by Jorgenson to the effect of crystal field upon inter-electronic repulsion between the 4f electrons and is related to covalence in the metal-ligand bond. The values of the bonding parameters are shown in Table 5. 2.

The positive and negative values of δ and $b^{1/2}$ for a complex correspond to covalent and ionic characters, respectively. A nephelauxetic ratio (β) of less than unity and positive values of Sinha's parameter (δ) and the bonding parameter ($b^{1/2}$) suggest the occurrence of some covalent character in the metal– ligand bond [7-9]. The small (δ%) values of the complexes indicate weak covalent bonding in the complexes. the small $\mathbf{b^{½}}$ values suggest weak participation of 4f orbital's in bonding.

Nephelauxetic ratio (β) :

$$\beta = \frac{\nu_c}{\nu_f}$$

(where ν_c & ν_f = wave numbers of f-f transition in spectra of metal complex and free metal ion in solvent)

Bonding Parameter ($b^{1/2}$) :

$$b^{1/2} = [\frac{1}{2}(1-\beta)]^{1/2}$$

Sinha's Covalency parameter (δ%)

$$\delta = \frac{1-\beta}{\beta} \times 100$$

Covalency angular overlap parameter (η):

$$\eta = \frac{1-\beta^{1/2}}{\beta^{1/2}}$$

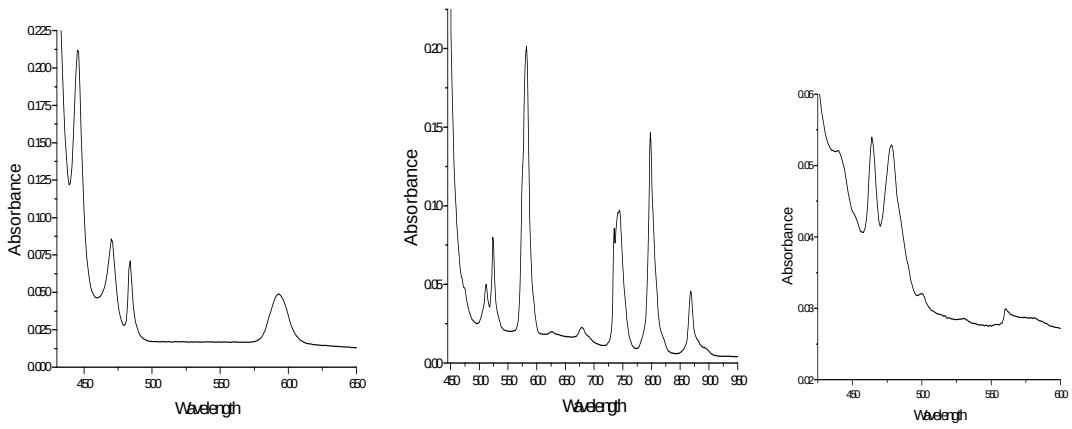

(A) (B) (C)

Fig. 5. 2 Electronic spectra of (A) Pr complex (B) Nd complex and (C) Sm Complex

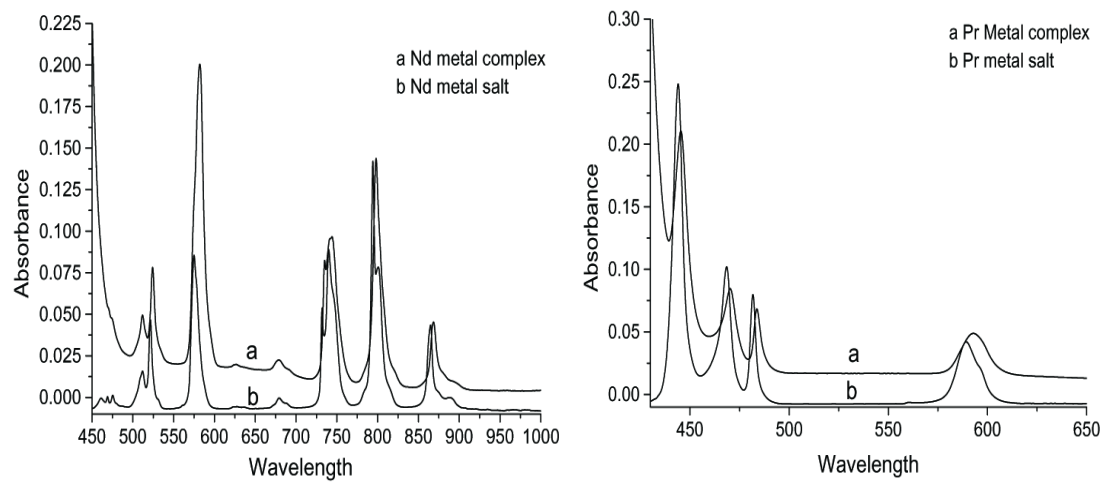

(A) (B)

Fig. 5.3 Electronic absorption spectra of (A) $Nd(NO_3)_3.6H_2O$ (red) & [$Nd(APAH)_2(NO_3)(H_2O)_2]2NO_3.\ 3H_2O$ (black) and (B)$Pr(NO_3)_3.6H_2O$ (red) & [$Pr(APAH)_2(NO_3)(H_2O)_2]2NO_3.3H_2O$ (black) in the visible region

Table 5.2 Electronic spectral data of the lanthanide complexes and related bonding parameter

Complexes	Frequency (cm^{-1})		Red shift (cm^{-1})	Assignment	β	(1-β)	$b^{1/2}$	δ	η
	Lanthanide Aqua ion	Lanthanide complexes							
$[Pr(APAH)_2(NO_3)(H_2O)_2].2NO_3.3H_20$	16,977	16,866	111	$^3H_4 \rightarrow {}^1D_2$	0.9935	0.0065	0.057	0.0065	0.0033
	20,746	20,661	85	$^3H_4 \rightarrow {}^3P_0$	0.9959	0.0049	0.0495	0.4932	0.0021
	21,367	21,276	91	$^3H_4 \rightarrow {}^3P_1$	0.9957	0.0043	0.0464	0.4319	0.0022
	22,522	22,466	56	$^3H_4 \rightarrow {}^3P_2$	0.9975	0.0025	0.0353	0.2506	0.0013
$[Nd(APAH)_2(NO_3)(H_2O)_2].2NO_3.3H_20$	11,560	11,511	49	$^4I_{9/2} \rightarrow {}^4F_{3/2}$	0.9958	0.0042	0.0458	0.4218	0.0021
	12,594	12,529	65	$^4I_{9/2} \rightarrow {}^4F_{5/2}$	0.9948	0.0052	0.051	0.5227	0.0026
	13,513	13,495	18	$^4I_{9/2} \rightarrow {}^4F_{7/2}$, $^3S_{3/2}$	0.9987	0.0013	0.0255	0.1302	0.0007
	17,391	17,182	209	$^4I_{9/2} \rightarrow {}^4G_{5/2}$, $^2G_{7/2}$	0.988	0.012	0.0775	1.21	0.006
	19,120	19,080	40	$^4I_{9/2} \rightarrow {}^4G_{7/2}$	0.9979	0.0021	0.0324	0.2104	0.0011
	19,569	19,535	34	$^4I_{9/2} \rightarrow {}^4G_{9/2}$	0.9983	0.0017	0.0292	0.1703	0.0009
$[Sm(APAH)_2(NO_3)(H_2O)_2].2NO_3.3H_20$	24,038	23,980	58	$^6H_{5/2} \rightarrow {}^6P_{5/2}$	0.9976	0.0024	0.049	0.2406	0.0012
	22,675	22,650	25	$^6H_{5/2} \rightarrow {}^4G_{9/2}$	0.9989	0.0011	0.0235	0.1101	0.0006
	21,598	21,594	4	$^6H_{5/2} \rightarrow {}^4I_{13/2}$	0.9998	0.0002	0.01	0.02	0.0001
	20,876	20,871	5	$^6H_{5/2} \rightarrow {}^4I_{11/2}$	0.9998	0.0002	0.01	0.02	0.0001
	20,040	20,000	40	$^6H_{5/2} \rightarrow {}^6G_{7/2}$	0.9980	0.0020	0.0316	0.2004	0.001

d. IR Spectroscopy

The FT- IR spectra of complexes in the region 4000-400 cm^{-1} are analyzed in comparison with that of the spectrum of metal free APAH (Fig 5.4). The characteristic IR peaks of APAH and its lanthanide complexes are given in Table 5.3. IR spectra of the five complexes are strikingly similar in relative positions and intensities of the peaks, which suggest a close structural relationship among the compounds. The vibrational bands observed in IR spectra of complexes 3430-3435 cm^{-1} region are assigned to *ν*(O-H) water molecule. The IR spectrum of the free ligand shows strong band at 1653 cm^{-1}, which is attributable to *ν*(C=O) stretching vibrations. The vibrational band at 1578 cm^{-1} can be assigned to the *ν*(C=N) of azomethine. In the IR spectra of lanthanide (III) complexes, the *ν*(C=O) and *ν*(C =N) shift by 14-26, 29–36. The shifts of the ν(C=O) and ν (C=N) vibrations of the bands towards lower wave numbers on complexation indicate participation of the carbonyl oxygen and azomethine nitrogen in coordination to the metal [9]. The vibrational band at 3198 cm^{-1} can be assigned to the *ν*(N-H) for the free ligand. The *ν*(N-H) band is observed in the range 3202-3220 cm^{-1} for the complexes. Observance of the *ν*(C=O) and *ν*(N-H) bands observed in the IR specta of complexes indicate that the APAH acts as neutral to tridentate ligand in the complex formation. The pyridine ring in-plane deformation mode observed at 623 cm^{-1} in the spectrum of APAH. The band shifts to 631 cm^{-1} in the spectra of lanthanide complexes indicating involvement of pyridine nitrogen donor atom in chelation[10].

The absorption bands assigned to the coordinated nitrate groups (*C*2v) are observed at about 1477 cm^{-1} (ν_1), 1295-1298 cm^{-1} (ν_4), 1027-1029 cm^{-1} (ν_2) and 819-

825 cm^{-1} (ν_3) for the nitrate complexes. The frequency separation [$\Delta\nu = \nu_1 - \nu_4$] between the asymmetric and symmetric stretching of this group can be made to distinguish between these binding states. The separation of the two bands is found in between 179–182 cm^{-1}. This observation suggests that NO_3^- acts as bidentate ligand [11, 12]. A new band is observed at 1384 cm^{-1} in IR spectra of complexes indicating the presence of ionic nitrate (D_{3h} symmetry), which is in agreement with the results of the conductivity experiments. The new bands in 416 - 423 and 541 - 546 cm^{-1} regions in the spectra of complexes are assigned to ν(Ln–O) and ν (Ln–N) vibrations respectively.

Table 5. 3 Infrared spectral data (cm^{-1}) for the APAH ligand and its lanthanide(III) complexes

Compound	**$\nu(O\text{-}H)_{water}$**	**$\nu(N\text{-}H)$**	**$\nu(C=O)$**	**$\nu(C=N)$**	**$\nu(NO_3^-)$**					
					ν_1	**ν_2**	**ν_3**	**ν_4**	**ν_0**	**ν_1-ν_4**
APAH	-	3198	1653	1578	-	-	-	-	-	-
$[La(APAH)_2(NO_3)(H_2O)_2]2NO_3.3H_2O$	3430	3202	1639	1542	1477	1029	825	1295	1384	182
$[Ce(APAH)_2(NO_3)(H_2O)_2]2NO_3.H_2O$	3431	3220	1638	1544	1477	1028	819	1295	1384	182
$[Pr(APAH)_2(NO_3)(H_2O)_2]2NO_3.3H_2O$	3433	3214	1639	1546	1477	1027	825	1298	1384	179
$[Nd(APAH)_2(NO_3)(H_2O)_2]2NO_3.3H_2O$	3432	3220	1636	1547	1477	1027	824	1298	1384	179
$[Sm(APAH)_2(NO_3)(H_2O)_2]2NO_3.2H_2O$	3435	3220	1627	1549	1477	1027	825	1298	1384	179

e. Thermo gravimetric (TG) analysis

Thermogravimetric analysis (TGA) gives information concerning the thermal stability of the complex and to decide whether the water and solvent molecules are in the inner and outer coordination sphere of the central metal [13]. The correlation between the different decomposition steps of Ln(III) complexes with the corresponding weight losses are discussed in terms of the proposed formula of the Ln(III) complexes.

The TGA results showed that the ligand L is thermally stable in the temperature range 30-145^{0}C and its decomposition starts at 145^{0}C and finishes at 254 °C with one decomposition step shown in Fig. 5.4. Thermal analysis carried out for La(III), Pr(III), Nd(III) complexes. The Ln(III) complexes showed similar thermal decomposition as shown in Fig. 5.5. The TGA curve of La(III) complex undergoes four-step changes.

The **first step** of decomposition (60-110° C) is due to the loss of three lattice water molecules with a weight loss of 7.3% which is consistent with theoretical value (7.02%). The **second step** of decomposition (210-243°C) is due to the loss of two coordinated water molecules with a weight loss of 4.52% is consistent with theoretical value (4.68%). The **third step** of decomposition (244-314° C) corresponds to loss of three nitrate ions with a weight loss of 24.12% is consistent with theoretical value (24.18%). The fourth stage of decomposition (315- 800) corresponds to the elimination and/or decomposition of ligand component. [14].

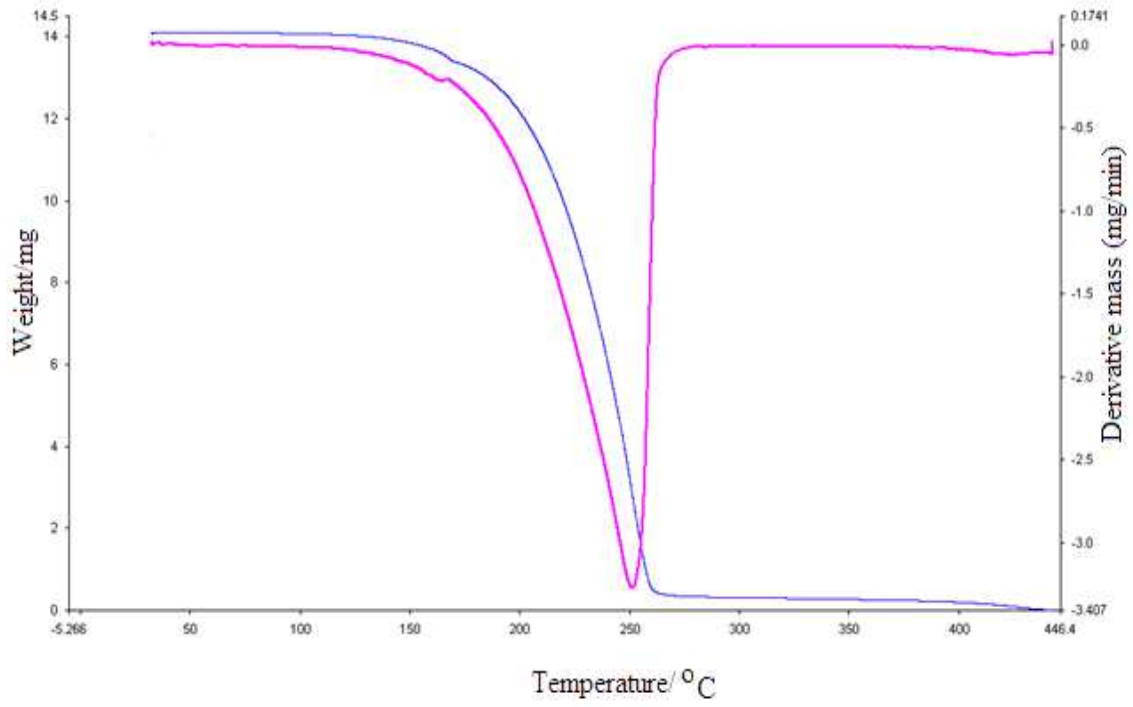

Fig. 5.4: TG and DTG curves for APAH ligand

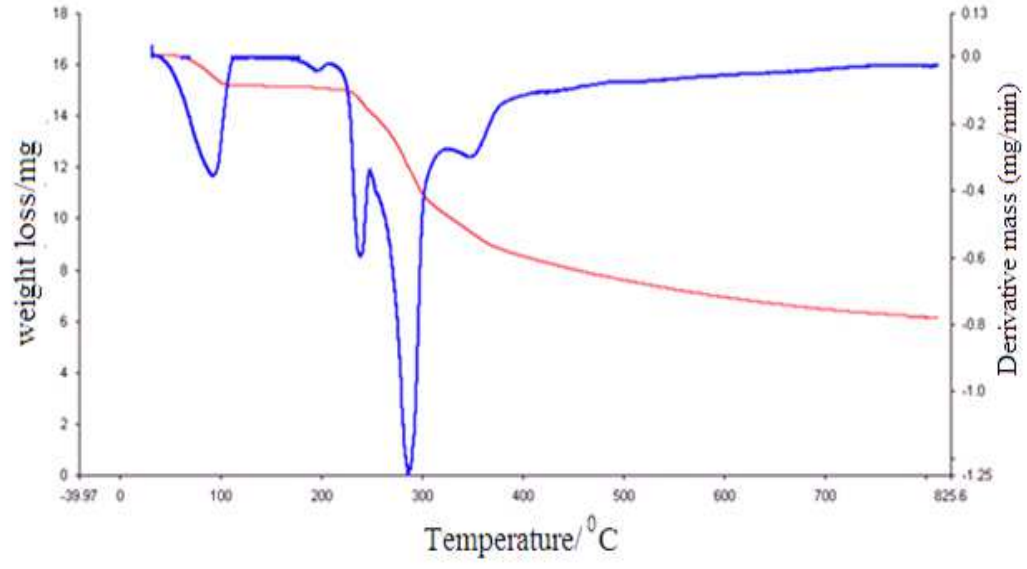

Fig. 5.5: TG and DTG curves for $[La(APAH)_2(NO_3)(H_2O)_2]2NO_3.3H_2O$

f. Description of the molecular structure of $[Ce(APAH)_2(NO_3)(H_2O)_2]2NO_3.H_2O$

The $[Ce(APAH)_2(NO_3)].2NO_3.H_2O$ compound crystallize in Triclinic, space group P-1 and the structure contains two monomeric complex cations i.e., $[Ce(APAH)_2(NO_3)(H_2O)_2]^{2+}$, 4 ionic nitrates and 2 water molecules in each unit cell, shown in Fig. 5.6. Crystal data and structure refinement parameters are shown in Table 5. 4. Selected bond lengths and bond angles are given in Tables 5.5 and Table 5. 6. ORTEP view of $[Ce(APAH)_2(NO_3)].2NO_3.H_2O$ together with the atom labeling scheme is shown in Fig. 5.7. Cerium atom is surrounded by 10- coordinated donor atoms. Six of them belong to two neutral tridentate ligands, two to the two mono dentate aqua ligand and two to the one bidentate nitrate group. The APAH ligand is coordinated to central metal atom to form two five membered rings. One five-membered chelate ring is formed with the pyridine nitrogen and the azomethine nitrogen and another five-membered chelate ring involves the azomethine nitrogen and carbonyl oxygen donor atoms.

Generally for 10- coordinate complexes, five polyhedra are considered [15]. They are (i) Bicapped square antiprism , (ii)Bicapped square prism, (iii) tetracapped trigonal prism, (iv) tetradecahedron and (v) pentagonal prism. In our case the coordination polyhedron around the Cerium atom is a distorted bicapped square antiprism, as shown in Fig. 5.8. The atoms of each APAH ligand are almost located on the same plane. Two APAH ligands are not in same plane. In Cerium complex O(2), O(4), N(4), O(7) define the one square face of the polyhedron and O(1), O(6), N(1), O(3) define the other. The two capping atoms are N(5) and N(2)

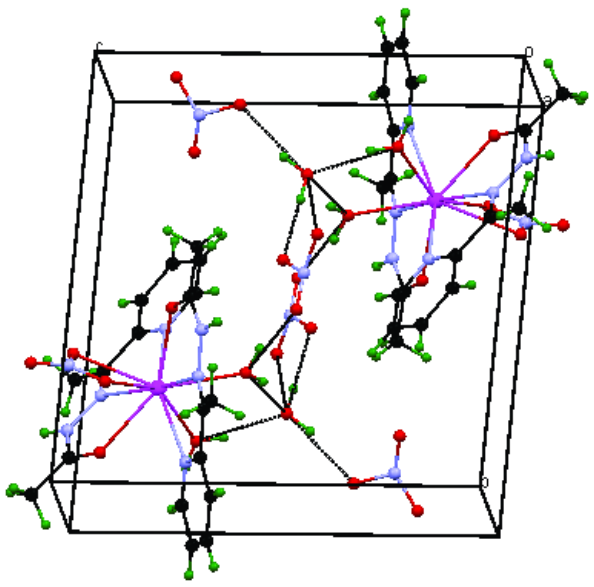

Fig 5.6: Unit cell structure of $[Ce(APAH)_2(NO_3)(H_2O)_2]2NO_3.H_2O$

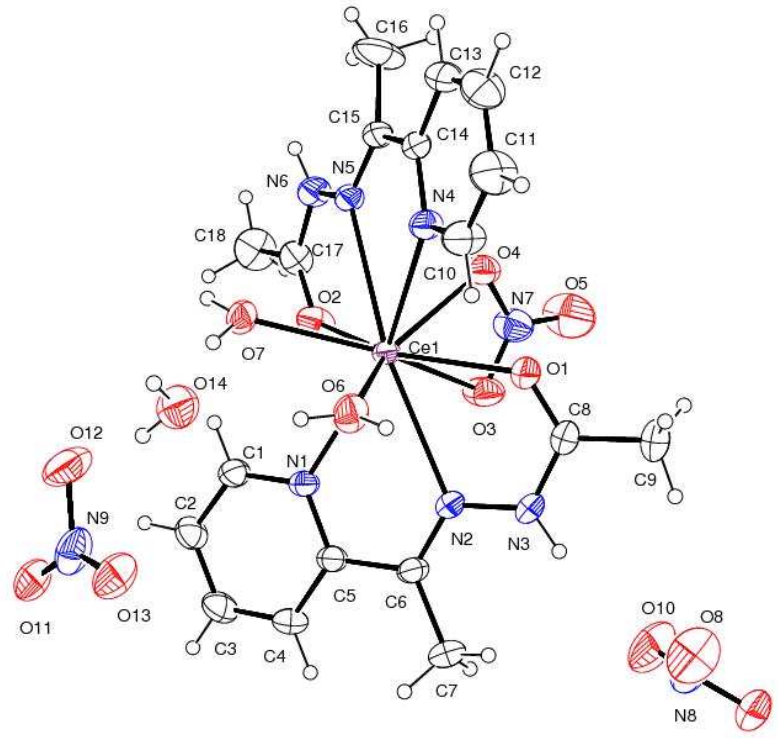

Fig 5.7: ORTEP view of $[Ce(APAH)_2(NO_3)(H_2O)_2]2NO_3.H_2O$

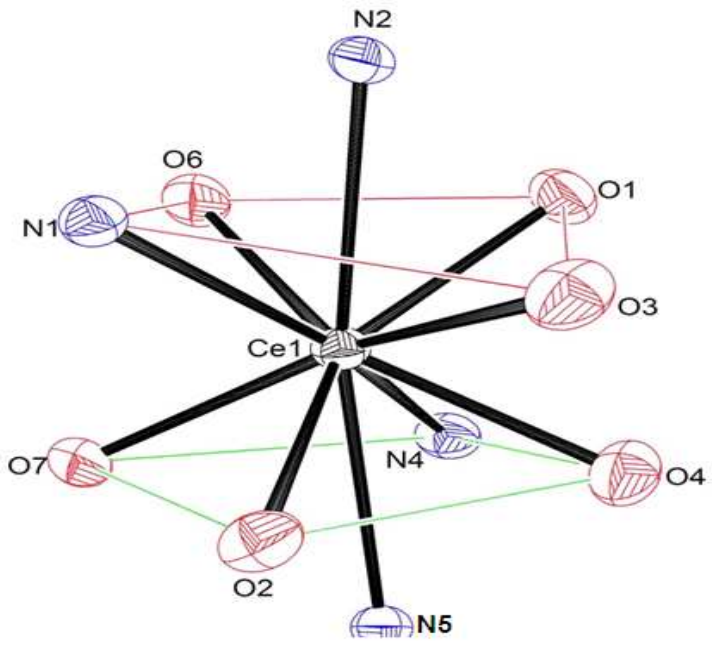

Fig 5.8: The coordination polyhedron around Cerium(III) ion

The Ce-O distances range between 2.472(2) and 2.619(6) Å with a mean value of 2.531 Å. Similarly the Ce-N distances range between 2.701 (2) and 2.731 (2) Å with a mean value of 2.717 Å. The Ce-O bond distances are shorter than Ce-N as can be expected for a hard oxygen donor bounded to a f-lanthanide ion [16]. The Ce-O (>C=O) bond lengths are 2.472(2) and 2.486(2), Ce-O(NO_3) bond lengths ranges between 2.513(2) and 2.619(6) Å. This suggest that Ce-O (>C=O) bond is slightly stronger than the Ce-O(NO_3) in the cerium complex. All Ce-O(water)distances [2.513(2) and 2.527(2) Å] are shorter than Ce-O(nitrate) distances [2.619(6) and 2.570 (13) Å]. Metal to ligand bond lengths are very short compare to previously reported ten coordinate cerium complex [17].

Bond lengths may be arranged in the series: **Ce-–O(carbonyl) < Ce–O(water) < Ce–O(nitrate)**

Table 5.4 Crystal data and structure refinement parameters for Ce and Sm Complexes

Complex	**Ce-APAH complex**	**Sm-APAH complex**
Empirical formula	$C_{18}\ H_{28}\ Ce\ N_9\ O_{14}$	$C_9\ H_{15}\ N_{4.5}\ O_{7.5}\ Sm_{0.5}$
Formula weight (M)	734.61	381.43
Temperature (*K*)	293(2)	293(2)
Wavelength (Mo Kα) (Å)	0.71073	0.71073
Crystal system,	Triclinic,	Triclinic,
Space group	*P-1*	*P-1*
Unit cell dimensions		
a(Å)	10.0739(4)	9.7844(4)
b(Å)	12.3384(4)	11.6495(4)
c(Å)	12.4353(5)	13.3022(5)
α(°)	83.611(2)	83.940(2)
β(°)	81.801(2)	77.589(2)
γ(°)	76.036(2)	78.460(2)
V(A^3)	1479.89(10)	1447.76(9)
Z	2	4
Calculated density *ρ*(Mgm^{-3})	1.649	1.750
Absorption coefficient μ (mm^{-1})	1.616	2.112
F(000)	738	766
Crystal size (mm)	0.30 x 0.25 x 0.20	0.25 x 0.20 x 0.15
Theta range for data collection (°)	2.10 to 25.00	2.17 to 25.00
Limiting indices	-11≤ *h* ≤11,	-11≤ *h* ≤11,
	-14≤ *k* ≤14,	-13≤ *k* ≤13,
	-14≤ *l* ≤14	-15≤ *l* ≤15
Reflections collected / unique	25285 / 5196 [R_{int} = 0.0293]	24820 / 5088 [R_{int} = 0.0244]
Completeness to *θ* (%)	99.9	99.8
Max. And min. transmission	0.7685 and 0.6326	0.7563 and 0.6132
Refinement method	Full-matrix least-squares on F^2	Full-matrix least-squares on F^2
Data / restraints / parameters	5196 / 223 / 504	5088 / 10 / 429
Goodness-of-fit on F^2	1.091	1.097
Final *R* indices [$I > 2s\sigma(I)$]	*R1* = 0.0224, *wR2* = 0.0579	*R1* = 0.0169, *wR2* = 0.0440
R indices (all data)	*R1* = 0.0257, *wR2* = 0.0613	*R1* = 0.0182, *wR2* = 0.0451
Largest diff. peak and hole($eÅ^{-3}$)	0.839 and -0.519	0.406 and -0.409

Table 5. 5 Selected Bond Lengths (Å) for the Structure of the Ce and Sm Complexes

Ce-APAH complex		**Sm-APAH complex**	
N(1)-Ce(1)	2.701(2)	N(1)-Sm(1)	2.6590(18)
N(2)-Ce(1)	2.731(2)	N(2)-Sm(1)	2.6269(18)
O(1)-Ce(1)	2.486(2)	O(1)-Sm(1)	2.4486(15)
N(4)-Ce(1)	2.714(2)	N(4)-Sm(1)	2.6332(18)
N(5)-Ce(1)	2.722(2)	N(5)-Sm(1)	2.6453(17)
O(2)-Ce(1)	2.472(2)	O(2)-Sm(1)	2.4066(16)
Ce(1)-O(3)	2.619(6)	O(3)-Sm(1)	2.5998(16)
Ce(1)-O(4)	2.570(13)	O(4)-Sm(1)	2.5478(17)
O(6)-Ce(1)	2.513(2)	O(6)-Sm(1)	2.4620(18)
O(7)-Ce(1)	2.527(2)	O(7)-Sm(1)	2.4742(19)

Table 5.6 - Selected Bond Angles (°) for the Structure of the Ce and Sm Complexes

Ce-APAH complex		**Sm-APAH complex**	
N(1)-Ce(1)-N(2)	57.97(7)	N(2)-Sm(1)-N(1)	59.41(6)
N(1)-Ce(1)-N(4)	153.97(8)	N(4)-Sm(1)-N(1)	135.33(6)
N(1)-Ce(1)-N(5)	126.89(7)	N(5)-Sm(1)-N(1)	120.18(6)
O(1)-Ce(1)-N(1)	117.68(7)	O(1)-Sm(1)-N(1)	120.52(5)
O(2)-Ce(1)-N(1)	72.29(7)	O(2)-Sm(1)-N(1)	74.03(6)
O(3)-Ce(1)-N(1)	85.79(14)	O(3)-Sm(1)-N(1)	68.03(6)
O(4)-Ce(1)-N(1)	129.0(2)	O(4)-Sm(1)-N(1)	70.22(6)
O(6)-Ce(1)-N(1)	79.29(8)	O(6)-Sm(1)-N(1)	144.36(6)
O(7)-Ce(1)-N(1)	77.07(7)	O(7)-Sm(1)-N(1)	78.20(7)

The Ce-N(py) distances [2.701(2) and 2.714(2)] and Ce-N (azomethane) distances [2.731(2) and 2.722(2)]. The difference may arise from constraints involved in chelate-ring formation or from the differing positions which N(py) and N(azo)

occupy in the coordination polyhedron, as well as from differential Ce → N back donation [18].

It is well known that pyridine based hydrazones can exist as two geometrical isomers based on azomethine, ***syn*** (Z) and ***anti*** (E), but in cerium complex, only the ***anti*** (E) isomer is possible show in Fig. 5.9. The torsion angles are C14–C15–N5–N6(179.29°), N5–N6–C17–O2(-7.11°), C5–C6–N2–N3(175.59°), N2–N3–C8–O1,(2.23°) suggest that the hydrazone adopts ***E*** conformation in coordination [19].

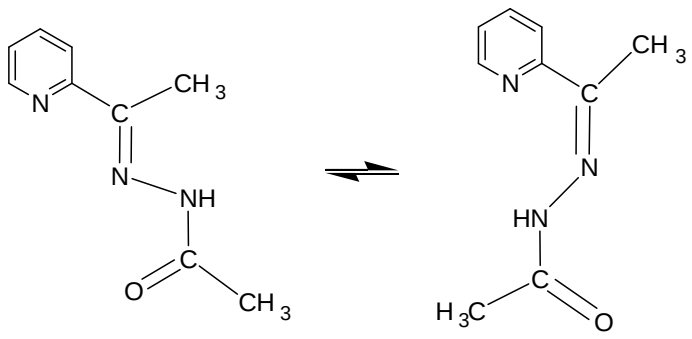

Fig 5.9: Geometrical Isomers of APAH

In cerium complex mainly three types of strong intermolecular hydrogen bonds are existing: (i) one is the N–H···O hydrogen bonding between the imine nitrogen and the oxygen atoms of non coordinate nitrate ion: (ii) the second is the O–H···N hydrogen bonding between the oxygen atoms of the coordinated water molecules and the nitrogen atoms of the non coordinate nitrate ion; (iii) the last one is the O– H···O hydrogen bonding between the oxygen atoms of the coordinate water molecules and the oxygen atoms of the non coordinate nitrate ion. Uncoordinated water molecules also participate in hydrogen bonding. Selected hydrogen bond lengths and bond angles are given in Table 5. 7. View of the hydrogen bond network is shown in Fig. 5.10.

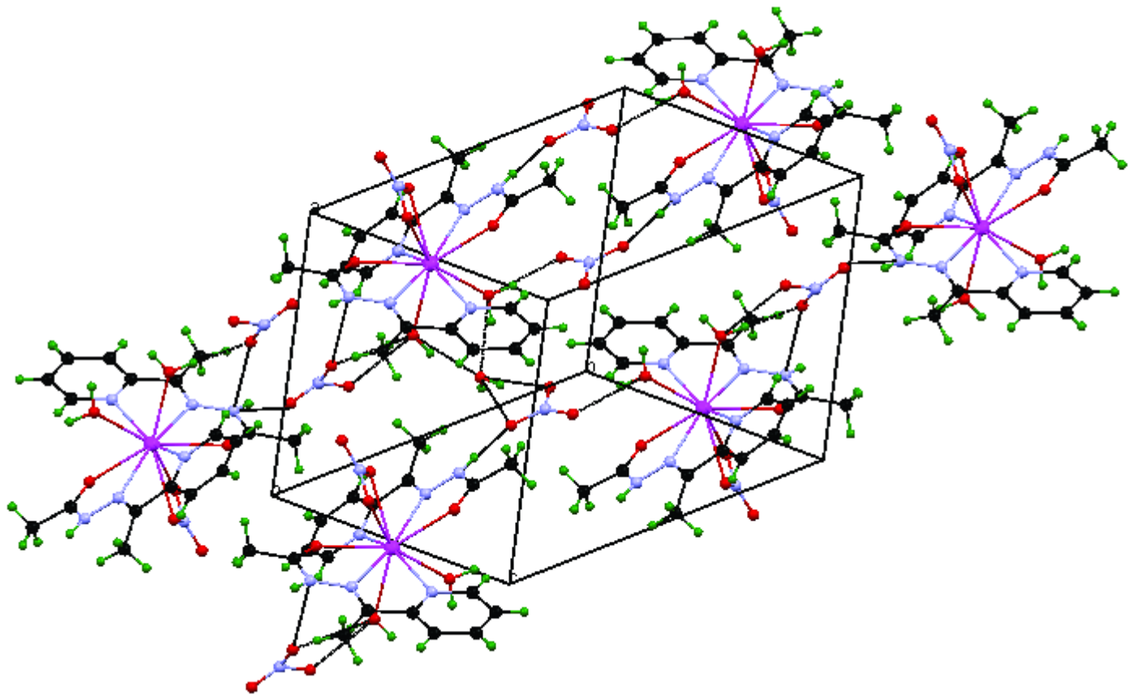

Fig 5.10: View of the Hydrogen bond network of $[Ce(APAH)_2(NO_3)(H_2O)_2]\ 2NO_3.H_2O$

Table 5. 7 Hydrogen bonds (Å) and bond angle (°)for the Ce-APAH complex

D-H...A	d(D-H)	d(H...A)	d(D...A)	<(DHA)
N(3)-H(3A)...O(10')	0.856(18)	2.14(3)	2.96(2)	161(2)
N(3)-H(3A)...O(10)	0.856(18)	2.33(3)	3.17(3)	165(3)
N(3)-H(3A)...O(8')	0.856(18)	2.53(4)	3.26(2)	144(3)
N(6)-H(6A)...O(13')[a]	0.867(19)	2.00(3)	2.858(18)	169(3)
O(6)-H(6C)...O(9')[b]	0.842(18)	2.07(4)	2.85(3)	154(4)
O(6)-H(6C)...O(9)[b]	0.842(18)	2.09(4)	2.86(3)	151(3)
O(6)-H(6C)...O(8)[b]	0.842(18)	2.20(3)	2.96(2)	149(4)
O(6)-H(6C)...N(8)[b]	0.842(18)	2.63(2)	3.464(4)	173(4)
O(7)-H(7H)...O(11)[c]	0.860(18)	1.93(2)	2.762(14)	161(4)
O(7)-H(7H)...O(12')[c]	0.860(18)	2.10(3)	2.876(17)	150(3)
O(7)-H(7H)...O(11')[c]	0.860(18)	2.39(3)	3.19(2)	155(4)
O(7)-H(7H)...N(9)[c]	0.860(18)	2.596(19)	3.453(4)	174(3)
O(7)-H(7H)...O(12)[c]	0.860(18)	2.64(3)	3.376(19)	144(3)

[a]Symmetry transformations used to generate equivalent atoms: x+1,y,z;

[b]Symmetry transformations used to generate equivalent atoms: -x+1,-y,-z ;

[c]Symmetry transformations used to generate equivalent atoms: -x+1,-y+1,-z+1

g. Description of the molecular structure of $[Sm(APAH)_2(NO_3)(H_2O)_2]2NO_3.2H_2O$

The $[Sm(APAH)_2(NO_3)].2NO_3.2H_2O$ compound crystallize in Triclinic, space group P-1 and the unit cell structure contains two monomeric complex cations i.e., $[Sm(APAH)_2(NO_3)(H_2O)_2]^{2+}$, 4 ionic nitrates and 4 water molecules in each unit cell, as shown in Fig. 5.11. Crystal data and structure refinement parameters are shown in Table 5. 4. Selected bond lengths and bond angles are given in Tables 5.5 and Table 5.6. ORTEP view of $[Sm(APAH)_2(NO_3)].2NO_3.2H_2O$ together with the atom labeling scheme used is shown in Fig. 5.12.

Samarium atom is surrounded by 10- coordinated donor atoms. Six of them belong to two neutral tridentate ligands, two to the two mono dentate aqua ligand and two to the one bidentate nitrate group. The APAH ligand is coordinated to central metal atom to form two five membered rings. One five-membered chelate ring is formed with the pyridine nitrogen and the azomethine nitrogen and another five-membered chelate ring involves the azomethine nitrogen and carbonyl oxygen donor atoms.

Generally for 10-coordinate complexes five polyhedra are considered [15]: that is (i) Bi capped square antiprism, (ii) Bicapped square prism, (iii) tetracapped trigonal prism, (iv) tetradecahedron and (v) pentagonal prism. In our case the coordination polyhedron around the Sm atom is a distorted bicapped square antiprism as shown in Fig. 5.13. The atoms of each APAH ligand are almost located on the same plane. Two APAH ligands are not in same plane. In samarium complex O(2), O(4),

N(4), O(6) define the one square face of the polyhedron and O(1), O(7), N(1), O(3) define the other. The two capping atoms are N(5) and N(2).

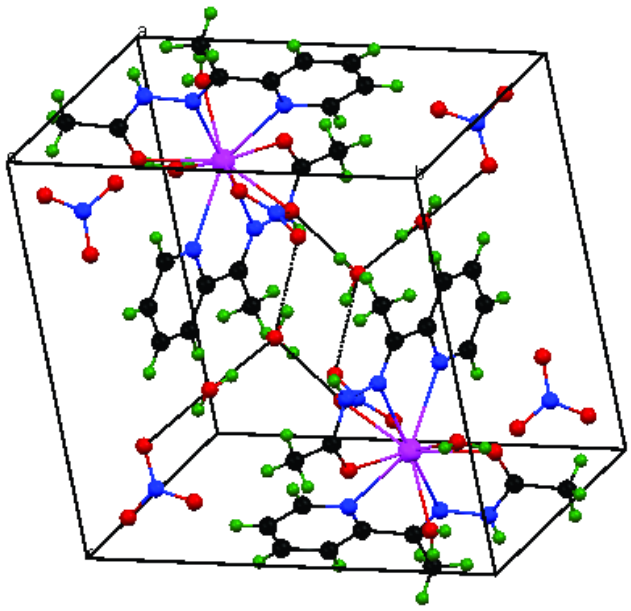

Fig 5 .11: Unit cell structure of $[Sm(APAH)_2(NO_3)(H_2O)_2]2NO_3.2H_2O$

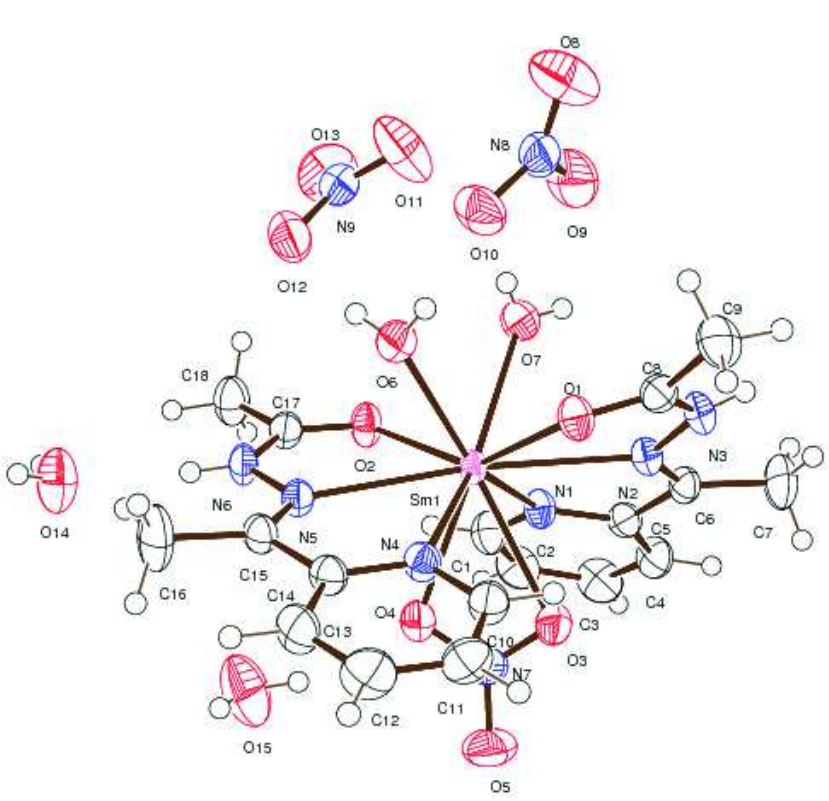

Fig 5.12: ORTEP view of $[Sm(APAH)_2(NO_3)(H_2O)_2]2NO_3.2H_2O$

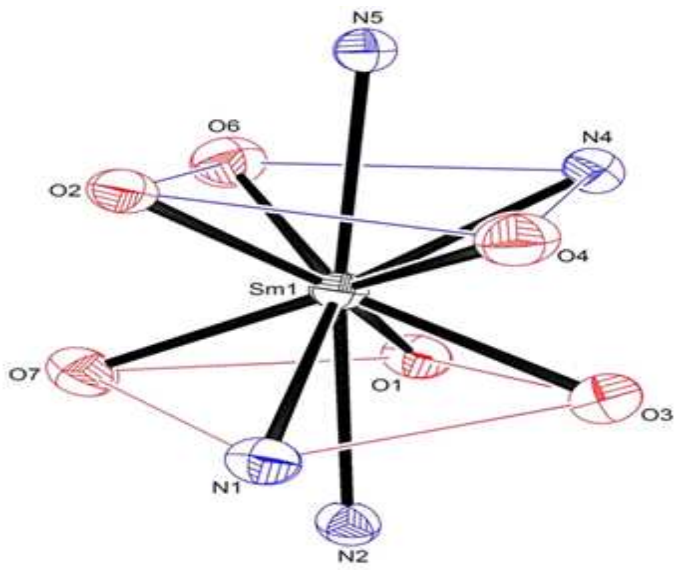

Fig 5.13: The coordination polyhedron around Samarium(III) ion

The Sm-O distances range between 2.4066(16) and 2.5998(16) Å with a mean value of 2.4898 Å. Similarly the Sm–N distances range between 2.6269(18) and2.6590 (18) Å with a mean value of 2.6433 Å. The Sm–O bond distances are shorter than Sm–N as can be expected for a hard oxygen donor bounded to a f-lanthanide ion [16]. The Sm-O (>C=O) bond distances are 2.4066(16) and 2.4486(15), Sm–O(NO_3) bond lengths ranges between 2.4620(18) and 2.5998(16). These data indicate that Sm-O (Carbonyl) bond is slightly stronger than the Sm–O(NO_3) in the Samarium complex. All Sm–O(water) distances are shorter than Sm–O(nitrate) distances.

Bond lengths order are Sm–O(carbonyl) < Sm–O(water) < Sm–O(nitrate)

The Sm–N(py) distances are [2.659(18) and2.6332(18)] and Sm–N (azo) distances are [2.6269(18) and 2.6453(17)]. the difference may arise from constraints involved in chelate-ring formation or from the differing positions which N(py) and N(azo) occupy in the coordination polyhedron, as well as from differential Sm → N back donation [18].

It is well known pyridine based hydrazones can exist as two geometrical isomers based on azomethine, ***syn*** (Z) and ***anti*** (E), but in samarium complex, only the ***anti*** (E) isomer is possible as shown in Fig. 5.9. The torsion angles [C14–C15–N5–N6(179.47°), N5–N6–C17–O2(-3.24°), C5–C6–N2–N3(175.19°), N2–N3–C8–O1,(2.12°)] suggest that the hydrazone adopts ***E*** conformation in coordination [19].

In samarium complex mainly two types of strong intermolecular hydrogen bonds are exist: one is the N–H···O hydrogen bonding between the imine nitrogen atom and the oxygen atom of non coordinate nitrate ion, the bond angle of which is 163(3)° (N(3)-H(3A)...O(11)[a]). The second one is the O–H···O hydrogen bonding between the hydrogen atoms of the coordinated water molecules and the oxygen atoms of the non coordinate nitrate ion. Uncoordinated water molecules also participate in hydrogen bonding with imine nitrogen atom. Selected hydrogen bond lengths and bond angles are given in Table 5.8. View of the hydrogen bond network is shown in Fig. 5.14.

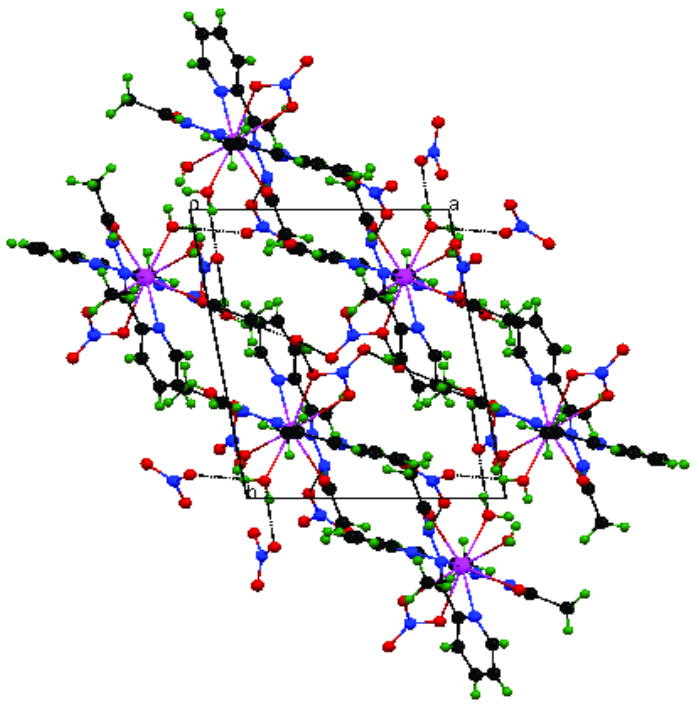

Fig 5.14: View of the Hydrogen bond network of $[Sm(APAH)_2(NO_3)(H_2O)_2]2NO_3.2H_2O$

Table 5. 8 Hydrogen bonds (Å) and bond angle(°)for the Sm complex

D-H...A	d(D-H)	d(H...A)	d(D...A)	<(DHA)
N(6)-H(6)...O(14)	0.78(3)	2.07(3)	2.835(3)	167(3)
N(3)-H(3A)...O(11)[a]	0.77(3)	2.20(3)	2.939(3)	163(3)
O(6)-H(6A)...O(10)	0.791(16)	1.971(18)	2.746(3)	166(3)
O(6)-H(6B)...O(12)	0.800(17)	2.007(19)	2.796(3)	169(4)
O(7)-H(7D)...O(9)[a]	0.77(4)	1.99(4)	2.751(3)	170(4)
O(7)-H(7E)...O(9)	0.69(4)	2.55(4)	3.087(3)	137(4)
O(7)-H(7E)...O(11)	0.69(4)	2.51(4)	3.111(4)	148(4)

[a]Symmetry transformations used to generate equivalent atoms:-x+2,-y,-z

The π–π stacking interaction between two pyridine rings [C10-C11-C12-C13-C14-N4] and [C10-C11-C12-C13-C14-N4] is found with the centroid–centroid separation of 3.744 Å, the shortest interplanar atom to atom separation is 3.731 Å

Comparison of cerium and samarium complexes

In samaraium complex bond lengths are smaller than the bond lengths of cerium complex. This may be due to less ionic radius of Sm(III). In cerium(III) complex ligand to metal bond length order is Ce–N(azomethine) > Ce–N(pyridine). This order is reversed in the Sm(III) complex. The polyhedron of cerium complex more deviated from bicapped square anti prism compared to samarium complex.

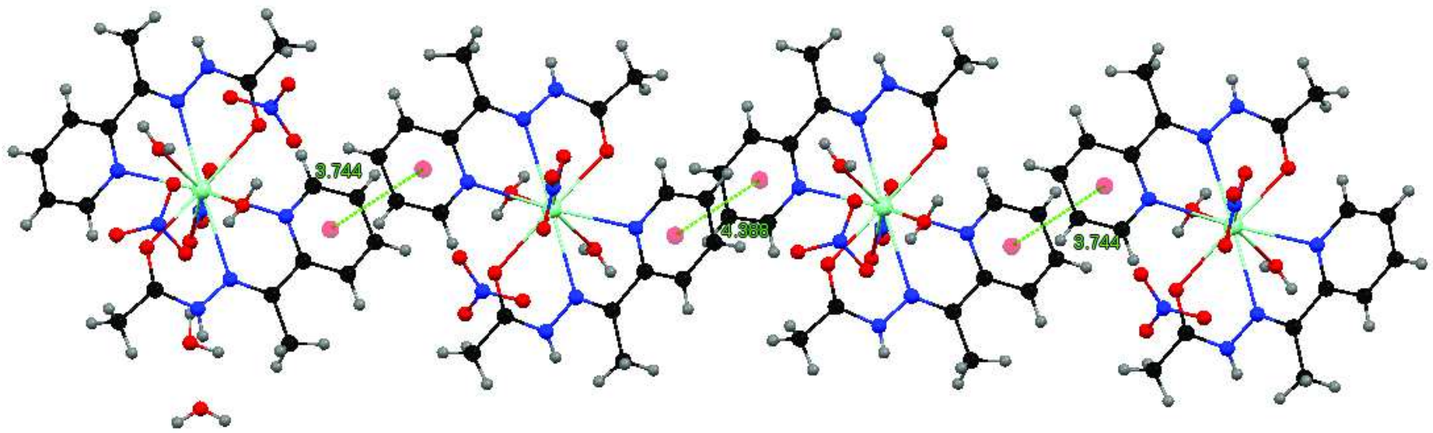

Fig 5.15: π…π stacking interactions of $[Sm(APAH)_2(NO_3)(H_2O)_2]2NO_3.2H_2O$

h. Hirshfeld surface analysis

The Hirshfeld surfaces represented by d_{norm} range of red (distances shorter than sum of vdW radii) through white to blue (distances longer than sum of vdW radii), shape index range of -1.0 (concave) through 0.0 (minimal surface) to +1.0 (convex) and 2-D fingerprint plots were calculated using Crystal Explorer 3.1 [20].

For each point on the Hirshfeld surface, two parameters are defined: d_e from the point to the nearest nucleus external to the surface and d_i is the distance from the point to the nearest nucleus internal to the surface. The normalized contact distance, dnorm, based on both de and di, and the vdW radius of the atom, given by an equation:

$$d_{norm} = \frac{d_i - r_i^{Vdw}}{r_i^{Vdw}} + \frac{d_e - r_e^{Vdw}}{r_e^{Vdw}} \qquad \ldots\ldots(1)$$

The Hirshfeld surface mapped over dnorm displays the intermolecular $OH_{(coordinate\ water)}\ldots O_{(ionic\ \ nitrate)}$ interactions as bright red , medium red colour is indicates $NH_{(imine)}\ldots O_{(ionic\ \ nitrate)}$ interactions and on the dnorm surface, a light red colour is indicates $CH_{(methyl)\ldots}O_{(ionic\ nitrate)}$ interactions in cerium complex shown in Fig 5.16.

The Hirshfeld surface mapped over dnorm displays the intermolecular $OH_{(coordinate\ water)}\ldots O_{(ionic\ \ nitrate)}$ interactions as bright red , medium red colour is indicates $NH_{(imine)}\ldots O_{(ionic\ \ nitrate)}$ interactions and on the dnorm surface, a light red colour is indicates $CH_{(methyl)\ldots}O_{(ionic\ nitrate)}$ interactions in samarium complex shown in Fig 5.16.

This decomposition enables separation of contributions from different interaction types, which overlap in the full fingerprint plot. In the 2-D fingerprint plots, two distinct spikes appear for O…H/H…O intermolecular interactions. The proportion of O…H/H…O interactions comprises 50.4%, 41.8% of the total Hirshfeld surfaces for

Ce, Sm complex respectively. The upper spike corresponding to the donor represents the O…H interactions and the lower spike being an acceptor represents the H…O interactions in the fingerprint plot (Fig 5.17). The decomposition of the fingerprint plot shows that C…H/H…C contacts comprise 10.1%, 9.4% of the total Hirshfeld surface area for Ce, Sm complex respectively. The region corresponds to all C–H…C interactions of which C–H…π appears in the fingerprint plot in a characteristic manner.

Hirshfeld surface of Ce complex does not show adjacent red and blue triangles on the shape-index surfaces (Fig. 5.16). This indicates absence of π-π stacking interactions. However some carbon-carbon interactions are present which comprises 2.5 % of the total Hirshfed surface area of Ce complex.

From the Hirshfeld surface, the adjacent red and blue triangles on the shape index surface shows that the π–π stacking interaction is almost identical to that of the crystal structure of samarium complex. The pattern of red and blue triangles in the same region of the shape index surface is another characteristic of π…π interactions. Blue triangles represent convex regions due to ring carbons of the molecule inside the surface, while red triangles represent concave regions due to carbons of the π-stacked molecule above it. The proportion of H…H interactions comprises 29.2%and 39.7% in 2D Fingerprint plot For Ce and Sm complexes.

Ce complex **Sm complex**

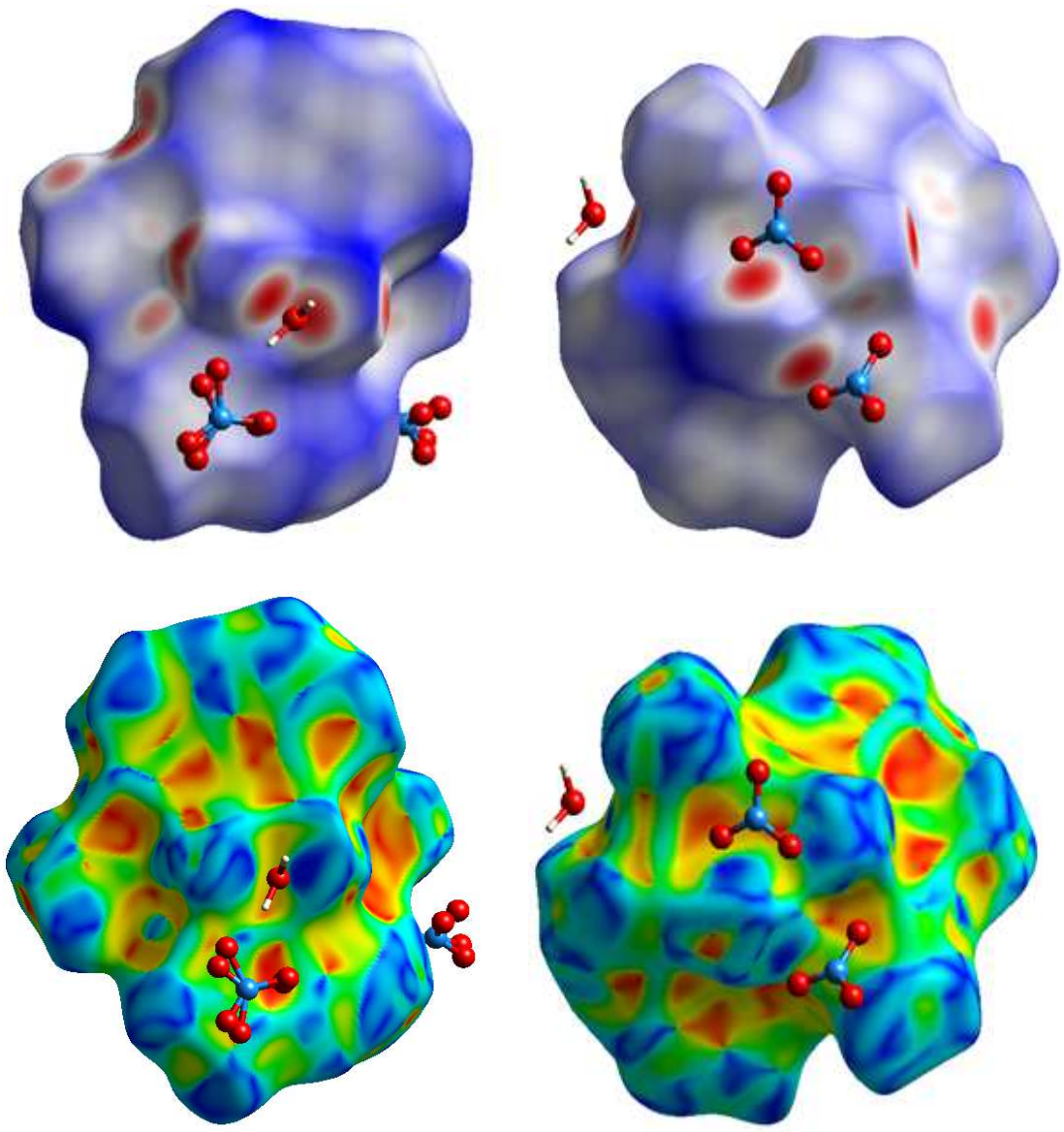

Fig 5.16: Hirshfeld surface mapped with (A) dnorm, (B) shape index for Ce and Sm complexes

Ce complex ***Sm complex***

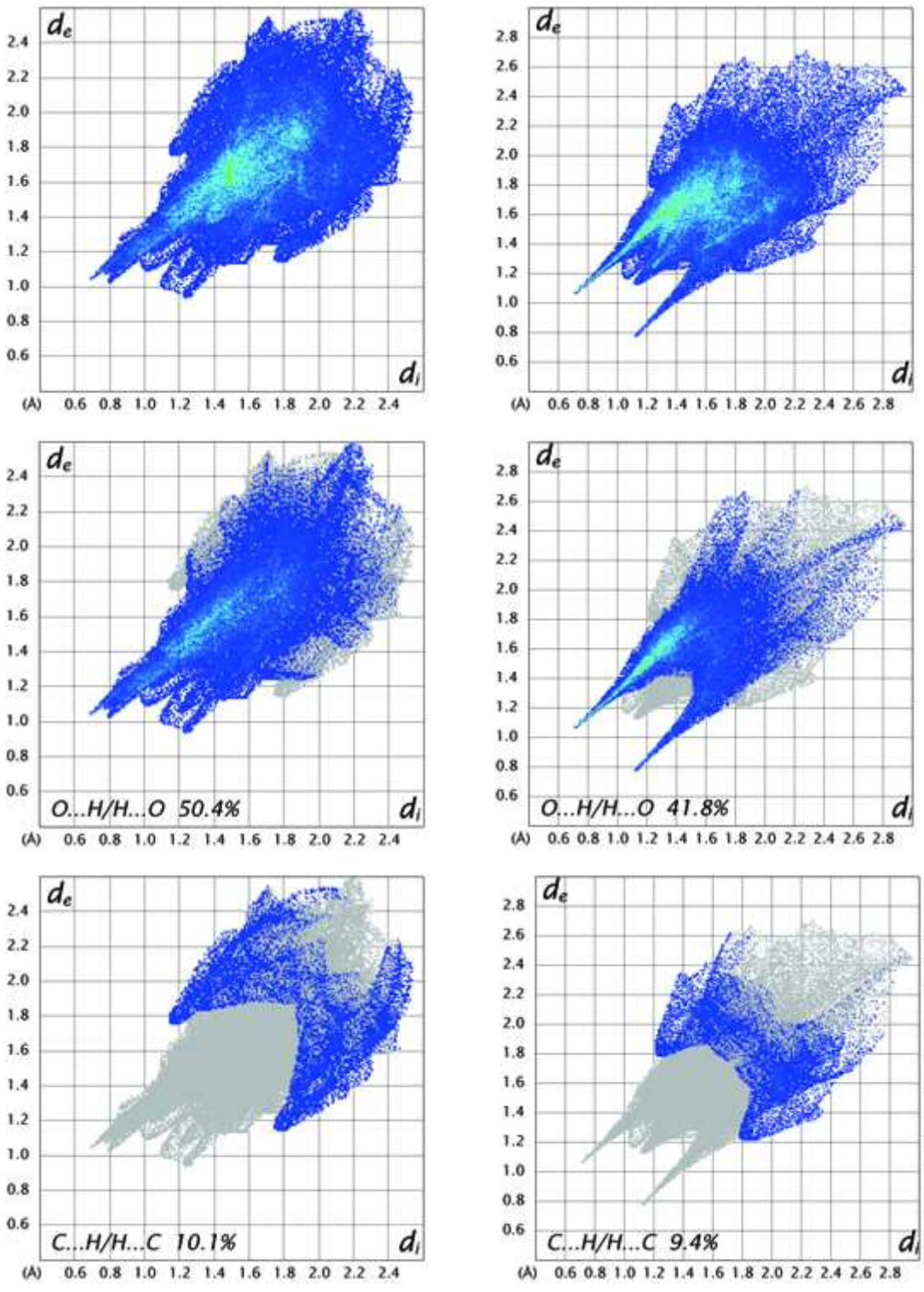

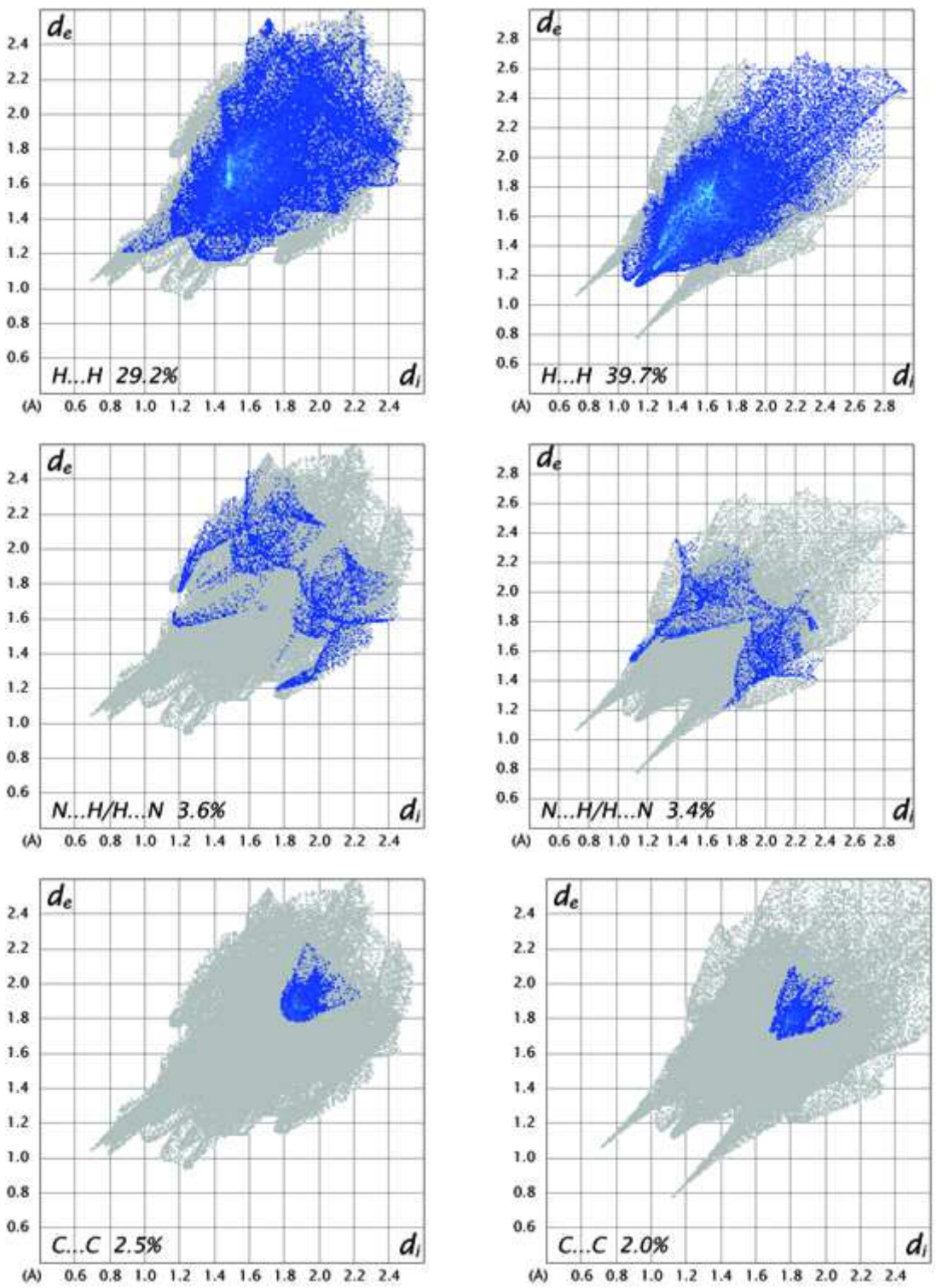

Fig 5.17: 2D fingerprint plots, full and resolved into OC/COOH/HO, CH/CH, H/H and C/C contacts showing percentages of contacts contributed to the total Hirshfeld surface area of Ce and Sm complex

i. Electrochemical studies

The redox behavior of the lanthanide(III) complexes has been investigated by cyclic voltammetry using 0.1M tetrabutylammonium hexaflourophosphate (TBAHEP) as supporting electrolyte. The cyclicvoltammograms of La(III), Ce(III). Pr(III), Nd(III) and Sm(III) gave irreversible waves. Their cathodic peak potentials are found to be a -0.78 [La(III)], -1.42 [Ce(III)], -0.966[Pr(III)],-1.05[Nd(III)] and -1.00[(Sm(III)] respectively. This is due to the reduction of Ln(III) to Ln(II). The cyclic voltammetric profiles of cerium(III) complex is given in Fig.5.18. A plot of i_p vs $\upsilon^{1/2}$(scan rate) is linear (Fig. 5.19) pointing towards diffusion controlled nature of reduction wave. In the reverse scan there is no anodic peak confirming the irreversible nature of electrode process. All these facts suggest the diffusion-controlled nature of the electrode process [21].

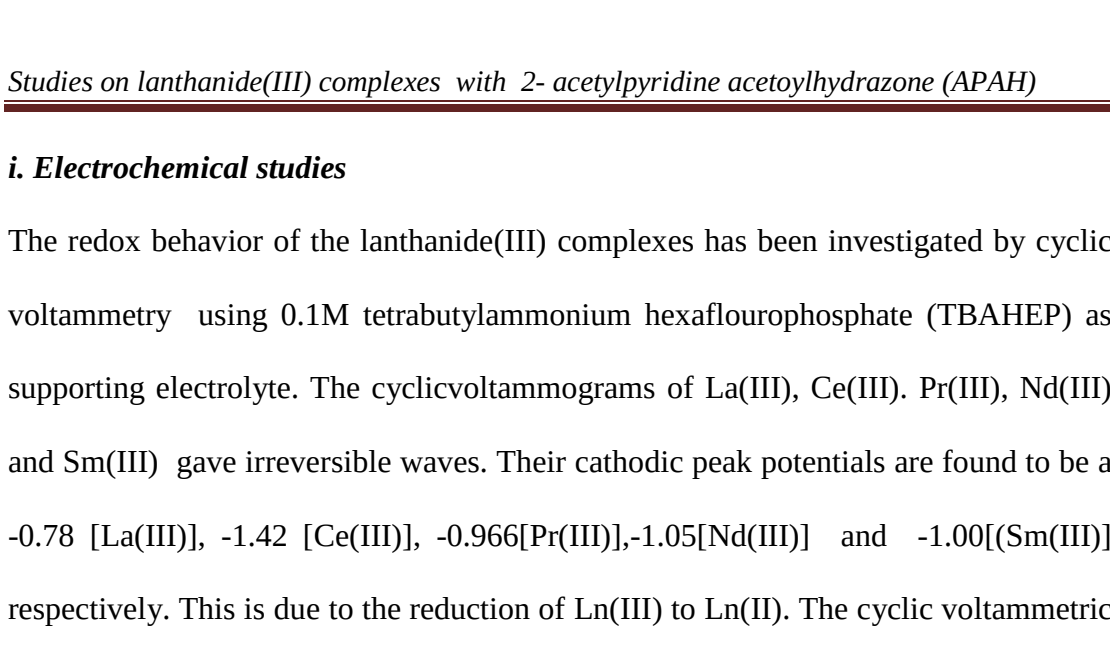

Fig 5.18: Cyclicvoltammetric profiles of the cerium complex at different scan rates 25-125 mV/s.

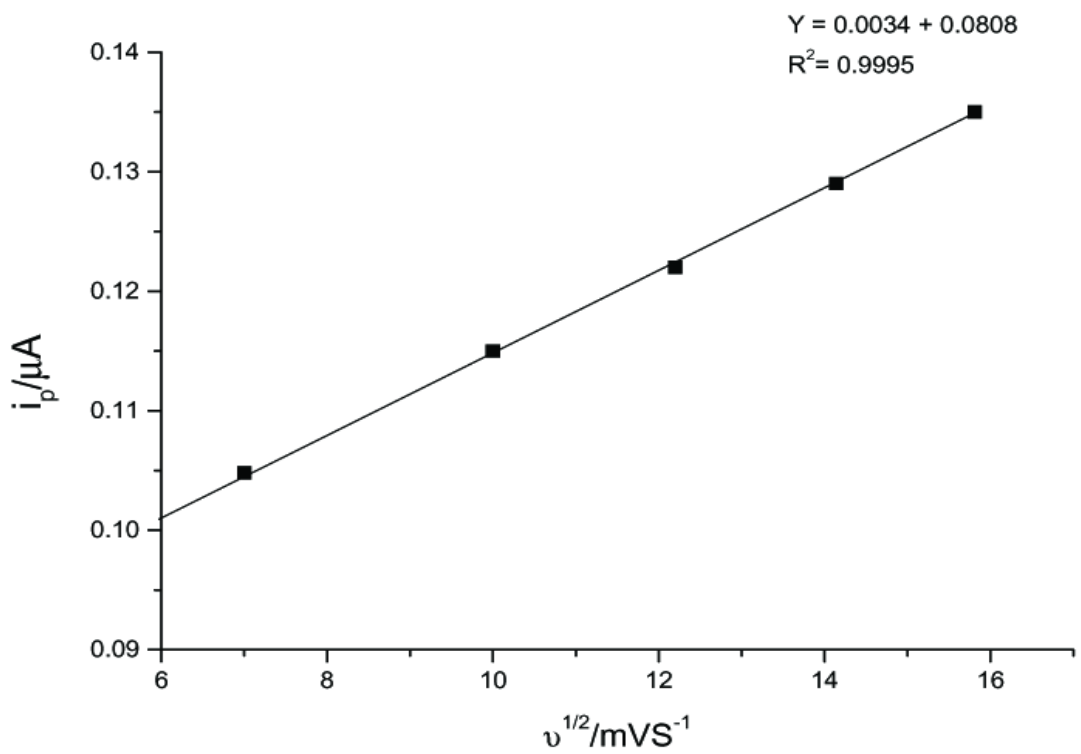

Fig 5.19: Plot of peak current vs scan rate for cerium complexes

j. DNA binding studies

Electronic absorption spectroscopy is an effective method for examining the interaction of DNA with metal complexes. Hyperchromic and hypochromic effects are the spectral changes when a complex interacts with DNA and forms a new complex. In general, a complex binding with DNA through intercalation usually results in hypochromism and bathochromism of the absorption band due to the intercalative mode involving a strong π- stacking interaction between the aromatic chromophore and base pairs of DNA [22]. The binding interaction of complexes with CT-DNA was monitored by comparing their absorption spectra with and without CT-DNA. All the complexes exhibit an intense absorption band in 285 - 289 nm region attributed to π→π* transition. Absorption spectra of

$[Ce(APAH)_2(NO_3)(H_2O)_2].2NO_3.H_2O$ in the absence and in presence of CT-DNA are shown Fig. 5.20. The metal-free hydrazone ligands show less DNA binding activity compare to lantahide-hydrazone complexes. The intrinsic binding constants (K_b), were determined by using the equation,

$$[DNA] / (\varepsilon_a-\varepsilon_f) = [DNA] / (\varepsilon_b-\varepsilon_f) + 1/ K_b(\varepsilon_b-\varepsilon_f) \quad \text{---------(2)}$$

Where [DNA] is the concentration of DNA in base pairs, ε_a, ε_b and ε_f are apparent extinction coefficient ($A_{obs}/[M]$), the extinction coefficient for the metal (M) complex in the fully bound form and the extinction coefficient for free metal (M) respectively. A plot of $[DNA] / (\varepsilon_a-\varepsilon_f)$ versus [DNA] gave a slope of $1/(\varepsilon_b-\varepsilon_f)$, and vertical intercept equal to $1/ K_b(\varepsilon_b-\varepsilon_f)$; K_b was calculated from these values. The binding constants (Table 5. 9) for lanthanide complexes are almost similar and independent of metal ion. This observation suggests that the complexes do not bind DNA via coordination (No direct Metal- DNA bond formation). On addition of DNA, the absorbance of the complexes decreases (hypochromism) and absorption maximum is shifted to higher wavelength (bathochromism). These observations suggest that the complexes bind DNA through intercalation/groove binding.

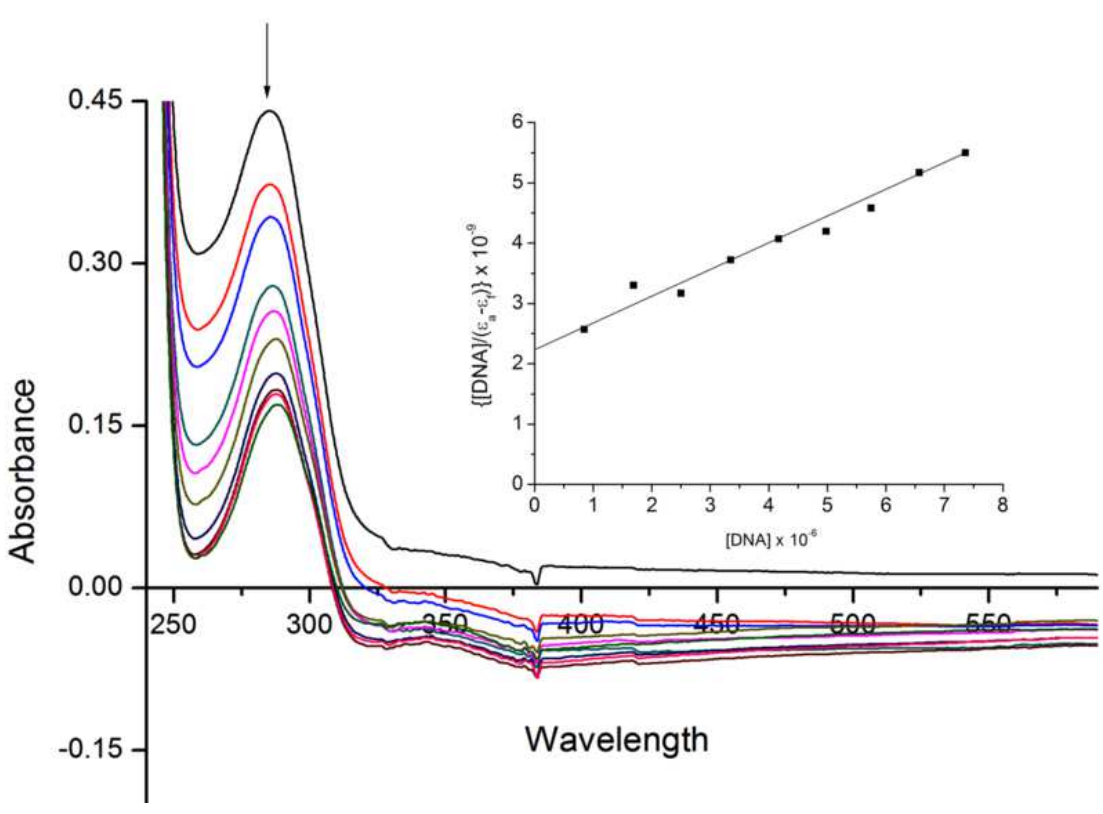

Fig 5.20: Absorption spectra of $[Ce(APAH)_2(NO_3)(H_2O)_2]2NO_3.H_2O$ in the absence and in the presence of increasing concentration of CT-DNA; top most spectrum is recorded in the absence of DNA and below spectra on addition of 10 μL DNA each time

Table 5. 9 Electronic absorption data upon addition of CT-DNA to the complexes

Complex	**λ_{max}(nm)**		**Δλ**	**H(%)**	**$K_b(M^{-1})$**
	Free	**bound**			
$[La(APAH)_2(NO_3)(H_2O)_2]2NO_3.\ 3H_2O$	285	286	1	+32.54	$2.98x10^5$
$[Ce(APAH)_2(NO_3)(H_2O)_2]2NO_3.\ H_2O$	286	289	3	+59.31	$2.13x10^5$
$[Pr(APAH)_2(NO_3)(H_2O)_2]2NO_3.\ 3H_2O$	285	286	1	+25.09	$2.34x10^5$
$[Nd(APAH)_2(NO_3)(H_2O)_2]2NO_3.3H_2O$	285	286	1	+27.51	$2.45x10^5$
$[Sm(APAH)_2(NO_3)(H_2O)_2]2NO_3.\ 2H_2O$	285	286	1	+26.83	$2.59x10^5$

k. DNA Cleavage studies

Nuclease activity of lanthanide complexes of 2-acetylpyridine acetoyl-hydrazone(APAH) has been studied by agarose gel electrophoresis using pBR 322 plasmid DNA in Tris-HCl/NaCl (50mM/5mM) buffer(pH-7) in the presence and in absence of H_2O_2 as an oxidant at micro molar concentration for 30 min incubation period at 37° C. The protocols of DNA cleavage are given in Chapter 2. In the presence of H_2O_2 the super coiled DNA (form I) is changed into nicked form (form II). Fig. 21 and Fig. 22 show the cleavage activity of lanthanide complexes. In the presence of H_2O_2 the complexes cleave DNA more effectively [lanes 6 and 8 in Fig. 5.21 and lanes 4 and 6 in Fig. 5.22], which may be due to the reaction of hydroxyl radical with DNA like Fenton mechanism [23]. These hydroxyl free radicals participate in the oxidation of the deoxyribose moiety, followed by hydrolytic cleavage of the sugar phosphate backbone [24]. The cleavage activity order (in the presence of hydrogen peroxide) is as follows

Ce complex > Pr complex > Nd complex > Sm complex > La complex

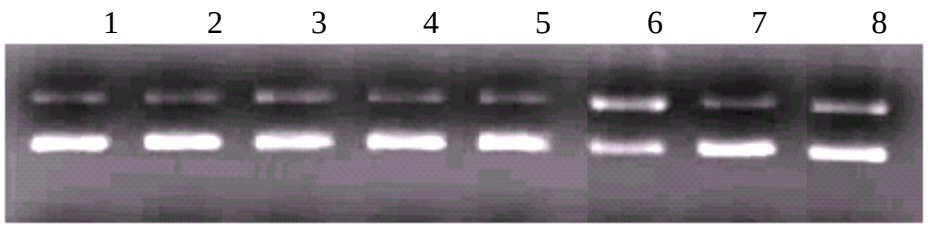

Fig 5.21: Agarose gel (0.8%) showing results of electrophoresis of 1 µl of pBR322 Plasmid DNA; 4 µl of Tris–HCl/NaCl (50 mM/5 mM) buffer (pH-7); 2 µl of complex in DMF($1x10^{-3}$ M); 11 µl of sterilized water; 2 µl of H_2O_2 (total volume 20 µl) were added, respectively, incubated at 37°C (30 min); **a** Lane 1: DNAcontrol; Lane 2: DNA control + H_2O_2; Lane 3: Lanthanum complex+ DNA ; Lane 4: Lanthanum complex + DNA + H_2O_2; Lane 5: Cerium complex+ DNA; Lane 6: Cerium complex+ DNA + H_2O_2; Lane 7:Samarium complex+ DNA; Lane 8: Samarium complex + DNA+H_2O_2.

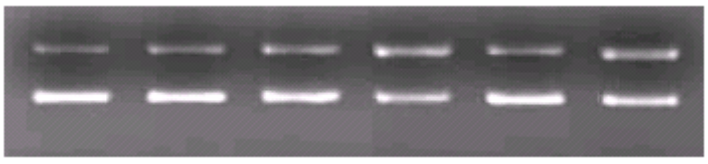

Fig 5.22: Agarose gel (0.8%) showing results of electrophoresis of 1 µl of pBR322 Plasmid DNA; 4 µl of Tris–HCl/NaCl (50 mM/5 mM) buffer (pH-7); 2 µl of complex in DMF($1x10^{-3}$ M); 11 µl of sterilized water; 2 µl of H_2O_2 (total volume 20 µl) were added, respectively, incubated at 37°C (30 min) Lane 1: DNA control; Lane 2: DNA control + H_2O_2; Lane 3: Praseodymium complex+ DNA; Lane 4: Praseodymium complex+ DNA + H_2O_2; Lane 5: Neodymium complex+ DNA; Lane 6: Neodymium complex+ DNA+H_2O_2;

Conclusions

La(III), Ce(III), Pr(III), Nd(III) and Sm(III) complexes of 2-Acetylpyridine acetoylhydrazone(APAH) have been synthesized and characterized. Physico-chemical and spectral studies reveal that the complexes have general formula [Ln $(APAH)_2(NO_3)(H_2O)_2]2NO_3.nH_2O$ (where Ln = La, Ce, Pr, Nd, and Sm). APAH acts as neutral tridentate ligand and NO_3^- acts as bidentate ligand. Two APAH ligands occupy six coordination sites, two aqua ligands occupy two coordination sites and one NO_3^- ligand occupies another two coordination sites to form 10- coordinate mono nuclear complexes. X-ray diffraction studies on $[Ce(APAH)_2(NO_3)(H_2O)_2]2NO_3.H_2O$ and $[Sm(APAH)_2(NO_3)(H_2O)_2]2NO_3.2H_2O$ confirm the suggested structures. Absorption titrations suggest that the complexes bind DNA through intercalation involving a strong π -stacking interaction between the aromatic chromophore (pyridine moiety) and base pairs of DNA. In presence of H_2O_2 lanthanide complexes cleave DNA more effectively which may be due to the reaction of hydroxyl radical with DNA. Thus the complexes cleave DNA via oxidative path.

The highlights of the present chapter are: (i) The structures of the complexes $[Ce(APAH)_2(NO_3)(H_2O)_2]2NO_3.H_2O$ and $[Sm(APAH)_2(NO_3)(H_2O)_2]2NO_3.2H_2O$ are determined by single crystal X-Ray diffraction studies, (ii) Spectral and bonding parameters are calculated in support of covalent character of metal- ligand bond, (iii) DNA binding and cleavage activities of the complexes are investigated. (iv) Solubility of present complexes in common organic solvents (Like Methanol, ethanol) is an attractive feature to develop chemotherapeutic drug.

Appendix A. Supplementary material

CCDC 917970 & CCDC 929565 contains the supplementary crystallographic data for Ce and Sm complexes. These data can be obtained free of charge via http://www.ccdc.cam.ac.uk/conts/retrieving.html, or from the Cambridge Crystallographic Data Centre, 12 Union Road, Cambridge CB2 1EZ, UK; fax: +44 1223 336 033; or e-mail: deposit@ccdc.cam.ac.uk.

References

1. E. Preshagen, E. Borbas, *Coord. Chem. Rev.* 273-274 **(2014)** 30.
2. C. M. G. Dos santos, J. H. Andrew, J. Q. Susan, T. Gunnlaugsson, *Coord. Chem. Rev.* 252 **(2008)** 2512.
3. B. Melanie, K. Lilan, J. L. Nicholas, *Chem. Soc. Rev.* 35 **(2006)** 557.
4. C. A. Barta, S.B. Krishna, J. Jesica, K.H. Thomspon, M.W. Kishore, O. Chris *Dalton Trans.* **(2007)** 5019
5. W. J. Geary, *Coord. Chem. Rev*. **7 (1971)** 81
6. A. Tavman, A. Cinarli, D. Gurbuz, *J. Iran. Chem. Soc.* 9 **(2012)** 815
7. S. P Sinha, *Spectrochim. Acta A* 22 **(1966)** 57
8. K. Iftikar, M. Sayeed, N. Ahmad, *Bull. Chem. Soc. Japan* 55 **(1982)** 2258
9. S. Prasad, R. K. Agarwal. A. Kumar, *J. Iran. Chem. Soc.* 8 **(2011)** 825.
10. K. Nakamoto, *Infrared and Raman Spectra of Inorganic and Coordination Compounds; John Wiley & Sons: New York,* (**1976)** Chapter 3.
11. N. F. Curtis, Y. M. Curtis, *Inorg. Chem.* 4 **(1964)** 804
12. P. Yan , W. Sun, G. Li, C. Nei, T. Gao, Z. Yue, *J. Coord. Chem.* 60 **(2007)** 1973.
13. A. A. A. Emara, B. A. E. Sayed, E. S. A. E. Ahmed, *Spectrochim. Acta A.* 69 **(2008)** 757.
14. X.M. Shi, R.R. Tang, G.L. Gu, K.L.Huang, *Spectrochim. Acta A* 72 **(2009)** 198.
15. S.P. SINHA, *Systematics and the properties of lanthanides, NATO ASI Series, Series C. Mathematical and Physical Sciences* No.109, p131 **(1982).**

16. M. Carcelli, S. Ianelli, P. Pelagatti, G. Pelizzi, D. Rogolino, C. Solinas, M. Tegoni, *Inorg. Chim. Acta.* 358 **(2005)** 903.

17. D. G. Paschalidis, M. Gdnaiec, *struct. Chem.* 15 **(2004)** 605.

18. J. Dan, S. Seth, S. Chakraborty, *Acta. Crystllogr. Sect. C* 45 **(1988)** 1018.

19. P. Sathyadevi, P. Krishnamoorthy, M. Alagesan, K. Thanigaimani, P.T. Muthiah , N. Dharmaraj, *Polyhedron* 31 **(2012)** 294.

20. S. K. Wolff, D. J. Grimwood, J. J. McKinnon, M. J. Turner, D. Jayatilaka, M. A. Spackman, University of Western Australia, 2012.

21. Ch. Jagadeeswara Rao, K. A. Venkatesan , K. Nagarajan, T. G Srinivasan, P. R. Vasudeva Rao, *J. Nucl. Mater.* 399 **(2010)** 81.

22. E. C. Long, J. K. Barton, Acc. Chem. Soc. Res. 23 **(1990)** 271.

23. Y. M. Song, J. P. Xu, L. Ding, Q. Hou, J. W. Liu, Z. L. Zhu, *J. Inorg. Biochem.* 103 **(2005)** 396.

24. W. K Pogozelski, T. D Tullius, *Chem. Rev.* 98 **(1998)** 1089.